remote sensing

MDPI

Technical Note

Reliability Evaluation of the Joint Observation of Cloud Top Height by FY-4A and HIMAWARI-8

Qinghui Li, Xuejin Sun * and Xiaolei Wang

College of Meteorology and Oceanography, National University of Defense Technology, Changsha 410000, China; liqinghui@nudt.edu.cn (Q.L.); wangxiaolei@nudt.edu.cn (X.W.)
* Correspondence: xuejin.s@nudt.edu.cn

Abstract: It is well known that the measurement of cloud top height (CTH) is important, and a geostationary satellite is an important measurement method. However, it is difficult for a single geostationary satellite to observe the global CTH, so joint observation by multiple satellites is imperative. We used both active and passive sensors to evaluate the reliability of joint observation of geostationary satellites, which includes consistency and accuracy. We analyzed the error of CTH of FY-4A and HIMAWARI-8 and the consistency between the two satellites and conducted research on the problem of missing measurement (Cloud-Aerosol Lidar and Infrared Pathfinder Satellite Observation (CALIPSO) has CTH data, but FY-4A/HIMAWARI-8 does not) of the two satellites. The results show that FY-4A and HIMAWARI-8 have good consistency and can be jointly observed, but the measurement of CTH of FY-4A and HIMAWARI-8 has large errors, and the error of FY-4A is greater than that of HIMAWIRI-8. The error of CTH is affected by the CTH, cloud optical thickness (COT) and cloud type, and the consistency between the two satellites is mainly affected by the cloud type. FY-4A and HIMAWARI-8 have the problem of missing measurement. The missing rate of HIMAWARI-8 is greater than that of FY-4A, and the missing rate is not affected by the CTH, COT and surface type. Therefore, although FY-4A and HIMAWARI-8 have good consistency, the error of CTH and the problem of missing measurement still limit the reliability of their joint observation.

Keywords: cloud top height; geostationary satellite; joint observation; missing measurement; FY-4A; HIMAWARI-8

check for updates

Citation: Li, Q.; Sun, X.; Wang, X. Reliability Evaluation of the Joint Observation of Cloud Top Height by FY-4A and HIMAWARI-8. *Remote Sens.* **2021**, *13*, 3851. https://doi.org/10.3390/rs13193851

Academic Editor: Simone Lolli

Received: 4 August 2021
Accepted: 23 September 2021
Published: 26 September 2021

Publisher's Note: MDPI stays neutral with regard to jurisdictional claims in published maps and institutional affiliations.

Copyright: © 2021 by the authors. Licensee MDPI, Basel, Switzerland. This article is an open access article distributed under the terms and conditions of the Creative Commons Attribution (CC BY) license (https://creativecommons.org/licenses/by/4.0/).

1. Introduction

Clouds have an important influence on the Earth's radiation balance [1–4]. The fifth Intergovernmental Panel on Climate Change (IPCC) report pointed out that the radiation effect of clouds is one of the biggest uncertain factors in evaluating future climate development and evolution [5,6], which mainly depends on CTH, COT, cloud phase state, etc. The Earth's climate system is driven by surface energy [2], which is composed of solar short-wave radiation and Earth's long-wave radiation, of which the Earth's long-wave radiation is significantly affected by the cloud top height [7–9]. Accurate measurement of cloud top height is very important for predicting climate change [10]. In addition, the cloud top height is also an important parameter in industries such as weather forecasting, artificial weather modification, and aviation. Its accurate acquisition is of great significance for the application of meteorological services [11,12]. Therefore, obtaining the cloud top height is a very important task.

At present, a variety of methods is used to detect cloud top height, forming a ground-based and space-based detection network, which can obtain global cloud top height data more comprehensively [13–18]. Among them, ground-based measurement is very important for continuous measurement of cloud top height, especially for thin cirrus clouds [19], but ground-based observation can only observe at fixed points, and the spatial resolution is low. Meteorological satellites can realize global cloud observation due to their large observation range, and satellite remote sensing provides observations over the ocean and

polar region where no ground-based station observations are available. Observations over the oceans provide precious information to initialize the numerical weather prediction models used to predict severe weather events such as hurricanes and tropical cyclones. Therefore, satellites have become the main methods of measuring the cloud top height. Meteorological satellite sensors are divided into active and passive categories. Active sensors such as Cloud-Aerosol Lidar with Orthogonal Polarization (CALIOP) mounted on CALIPSO and Cloud Profiling Radar (CPR) mounted on CLOUDSAT can measure cloud top height [20–24]. Both CALIPSO and CLOUDSAT are in the low Earth orbit (LEO). Active remote sensing satellites have global observation capabilities, but it is difficult to continuously observe a certain location for a long time, with low time resolution and a small field of view. In contrast, geostationary satellites equipped with passive sensors cover a large area and can continuously observe fixed locations. Instruments on geostationary satellites such as Advanced Geostationary Radiation Imager (AGRI) of FY-4A, Advanced Himawari Imager (AHI) of HIMAWARI and Advanced Baseline Imager (ABI) of Geostationary Operational Environmental Satellite (GOES) have been widely used. The cloud top height detection methods of passive remote sensing satellites mainly include the thermal infrared method and CO_2 slicing method [25–27]. However, the thermal infrared method does not consider the influence of radiation under the cloud, so it is not applicable to thin clouds. In addition, the thermal infrared method needs to rely on the temperature profile to convert the brightness temperature into the cloud top height, and the measurement error of the temperature profile will cause a cloud top height measurement error. For the CO_2 slicing method, when the target cloud is a fragmented cloud or a thin cirrus cloud, the radiation difference between the radiation measured by the detection channel and the clear sky may be smaller than the instrument noise, making the method inapplicable.

Although geostationary satellites cover a large area, each geostationary satellite can only observe a specific area, and it is difficult to observe the global cloud top height. In order to observe the global cloud top height, the joint observation of multiple geostationary satellites is a very necessary task. However, the joint observation of multiple geostationary satellites still has two problems. First, the performance of sensors on different satellites and the algorithm for inverting cloud top height are different, and the accuracy of measuring cloud top height is low. Therefore, before conducting joint observation, it is necessary to evaluate the accuracy of the cloud top height measured by the geostationary satellite and the consistency of cloud top height between the geostationary satellite. Second, the satellite's observations have the missing values. Therefore, it is necessary to combine the active sensor to evaluate the problem of the missing measurement of the cloud top height by the geostationary satellite.

FY-4A is the first geostationary satellite of China's next generation [28], and HIMAWARI-8 is a Japanese geostationary satellite [29]. Both can provide cloud top height products, and the detection range of the two has a large intersection area, so we chose FY-4 and HIMAWARI-8 to evaluate the reliability of joint observation of cloud top height and evaluate the performance of FY-4 and HIMWARI-8 to measure cloud top height to provide the basis for the next step of joint observation of cloud top height by geostationary satellites.

2. Data

In this paper, FY-4 and HIMAWARI-8 are evaluated for the reliability of joint observation of cloud top height. There are two main aspects. One is the accuracy and difference of cloud top height of HIMAWARI-8 and FY-4, and the other is the problem of missing measurements of HIMAWARI-8 and FY-4. Therefore, we used the cloud top height data of the three satellites CALIPSO, HIMAWARI-8 and FY-4A, as well as other auxiliary parameters such as cloud phase, cloud type, optical thickness, cloud layer number and surface type.

FY-4A is the first geostationary satellite of China's next generation. It can provide cloud top height data from 23.5° to 185.8° in longitude and from −80.8° to 80.8° in latitude. We use FY-4A's full-disk cloud top height product with a time resolution of about 15 min and a horizontal resolution of 4 km. HIMAWARI-8 is a Japanese geostationary satellite that

can provide cloud top height and cloud type data from 80° to 200° in longitude and from −60° to 60° in latitude, with a time resolution of 10 min and a spatial resolution of 5 km.

The CALIOP lidar mounted on CALIPSO can more accurately measure the cloud top height. CALIPSO's cloud product data can be used to evaluate the measurement accuracy of the cloud top height of HIMAWARI-8 and FY-4A and the problem of missing measurement. The CALIPSO data used in this study can provide the cloud top height, optical thickness, cloud layer number, cloud phase, surface type and other data of clouds below 20 km.

Table 1 lists the center wavelength and bandwidth of the channels used in the CTH retrieval algorithm by FY-4A and Himawari-8.

Table 1. FY-4A/AGRI and Himawari-8/AHI bands used in the CTH retrieval (FWHM: full width at half-maximum).

	Central Wavelength (μm)	Bandwidth (FWHM; μm)
HIMAWARI-8	10.8	1.0
	12.0	1.0
	13.5	0.6
FY-4A	11.2	0.67
	12.4	0.97
	13.3	0.56

FY-4A uses a combination of 10.8 μm, 12.0 μm and 13.5 μm to retrieve the cloud top height [28]. The CO_2 slicing method is applied to the 13.5 μm, the split window method is applied to the 10.8 μm and 12 μm, and the cloud top height is retrieved by combining with the optimal estimation method [30–32]. The cloud top height retrieval method of HIMAWARI-8 is similar to the Integrated Cloud Analysis System (ICSA) [29]; it also uses the CO_2 slicing method and the split window method combined with the optimal estimation to obtain the cloud top height [33]. CALIPSO is equipped with a dual-band (532nm and 1064 nm) lidar with orthogonal polarization detection capability, which can accurately reflect the extinction coefficient profile of clouds and aerosols and their distribution heights through backscattering, which can effectively distinguish ice cloud and water cloud and obtain the geometric height of the cloud [34–36].

The FY-4A and HIMAWARI-8 have a large crossover range. Therefore, the cloud top height data of CALIPSO can be used to evaluate the difference in the cloud top height detected by the two geostationary satellites and the reliability of the joint observation of the cloud top height. This article selects the data from July 2019 for analysis. The matching range of FY-4A and HIMWARI-8 is 80° to 180° in longitude and −60° to 60° in latitude.

3. Results

3.1. The Measurement Accuracy of FY-4A and HIMAWARI-8 and the Difference between the Two

Both FY-4A and HIMAWARI-8 are equipped with visible light infrared radiation imagers, and the accuracy of the cloud top height inversion is poorer than that of CALIPSO's lidar. In the joint observation of the geostationary satellite, the accuracy of the geostationary satellite and the consistency of the measurement results of the geostationary satellite need to be evaluated.

In order to evaluate the accuracy of cloud top height of FY-4A and HIMAWARI-8 and the difference between the two, we used cloud top height deviation (ΔCTH), the mean bias error (MBE) and standard deviation (Std), which are defined as shown in Equations (1)–(3):

$$\Delta CTH_i = X_i - Y_i \tag{1}$$

$$\mathrm{MBE} = \frac{\sum_{i=1}^{N} (X_i - Y_i)}{N} \tag{2}$$

$$Std = \sqrt{\frac{\sum_{i=1}^{N} (\Delta CTH_i - MBE)^2}{N-1}} \quad (3)$$

where X and Y are the cloud top height of two satellites, N is the number of samples. MBE can be used to evaluate the measurement accuracy of FY-4A and HIMAWARI-8 and the consistency of the measurement results between the two satellites.

When making the comparison, we considered a variety of scene types, such as multi-layer clouds and single-layer clouds, ice clouds and water clouds, land and ocean. Cloud scenarios are all determined by CALIPSO. Since the input radiation values of the FY-4A and HIMAWARI-8 cloud top height retrieval algorithms are thermal infrared radiance, there is no need to distinguish day and night.

Figure 1 shows the ΔCTH frequency distribution and MBE of all samples, multi-layer clouds and single-layer clouds between different satellites. Figure 1a,b are the comparison results of FY-4A and HIMAWARI-8 with CALIPSO. The MBE of FY-4A single-layer cloud is −3.49 km, the MBE of a multi-layer cloud is −6.6 km. The MBE of HIMAWARI-8 single-layer cloud is −1.84 km, the MBE of multi-layer cloud is −4.94 km. It can be seen from the figure that the measurement results of FY-4A and HIMAWARI-8 are significantly smaller than that of CALIPSO, and the error of multi-layer clouds is larger than that of single-layer clouds. In addition, the frequency distribution of single-layer clouds and multi-layer clouds is significantly different. Figure 1c is the comparison result between FY-4A and HIMAWARI-8. It can be seen from the figure that the MBE of a single-layer cloud is −1.54 km, and the MBE of a multi-layer cloud is −0.79 km. The MBE of a multi-layer cloud is smaller than that of a single-layer cloud, and both are small. At the same time, the ΔCTH frequency distribution of single-layer clouds and multi-layer clouds is basically the same.

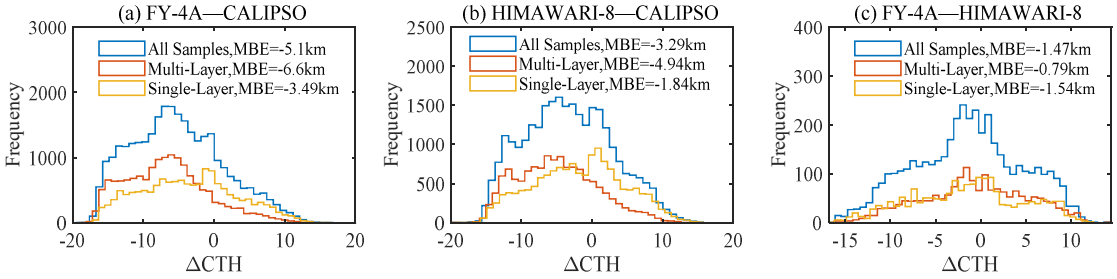


Figure 1. The ΔCTH frequency distribution of all samples, multi-layer clouds and single-layer clouds between different satellites. (**a**) FY-4A–CALIPSO, (**b**) HIMAWARI-8–CALIPSO, (**c**) FY-4A–HIMAWARI-8.

Figure 2 shows the ΔCTH frequency distribution and MBE of ice cloud and water cloud (single layer) between different satellites. Figure 2a,b show the comparison results of FY-4 and HIMAWARI-8 with CALIPSO. The MBE of the ice cloud of FY-4A is −8.25 km, the MBE of the water cloud is 0.3 km, the MBE of the ice cloud of HIMAWARI-8 is −6.19 km, and the MBE of the water cloud is −3.0 km. It can be seen from the figure that the MBE of the ice cloud of FY-4A and HIMAWARI-8 is much larger than that of the water cloud, and the MBE of the water cloud of FY-4A is smaller than that of HIMAWARI-8, and the MBE of the ice cloud of FY-4A is larger than that of HIMAWARI-8. The frequency distribution of ΔCTH between the ice cloud and water cloud of FY-4A and HIMAWARI-8 is obviously different, and the frequency distribution of the two satellites is similar. It can be seen from Figure 2b that the distribution of the water cloud has a bimodal distribution, but combined with the distribution of other scenarios of HIMAWARI-8, we think this is just an accidental situation. Figure 2c shows the comparison result between FY-4A and HIMAWARI-8. It can be seen from the figure that the MBE of the ice cloud = −1.03 km, and the MBE of the water cloud = −2.54 km. The consistency of the ice cloud between two satellites is better than that of the water cloud, and the range of ΔCTH of the ice cloud is slightly larger than the water cloud.

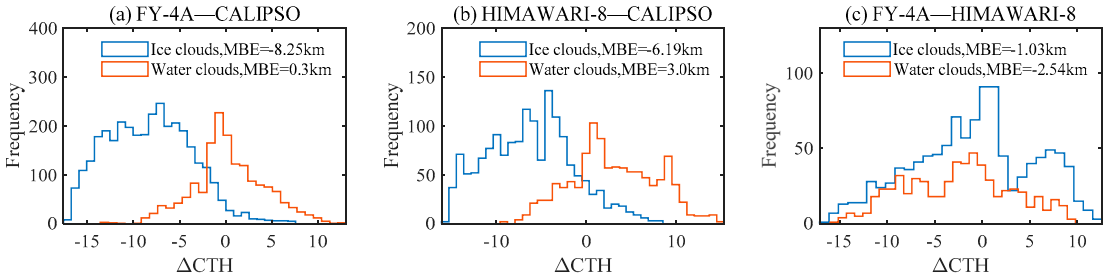


Figure 2. The ΔCTH frequency distribution of ice clouds and water clouds between different satellites. (**a**) FY-4A–CALIPSO (**b**) HIMAWARI-8–CALIPSO (**c**) FY-4A–HIMAWARI-8.

The results of Figures 1 and 2 show that the errors of FY-4A and HIMAWARI-8 are both large. Among them, the error of multi-layer clouds is greater than that of single-layer clouds, and the error of ice clouds is greater than that of water clouds. The error of FY-4A is larger than that of HIMWARI-8, but the MBE between FY-4A and HIMAWARI-8 is small.

It can be seen from the above analysis that FY-4A and HIMAWARI-8 have good consistency and can be jointly observed, but the error of FY-4A and HIMAWARI-8 limits the reliability of joint observation. Therefore, analysis of factors affecting cloud top height measurement and the consistency between FY-4A and HIMAWARI-8 is necessary to improve the reliability of joint observation of FY-4A and HIMAWARI-8.

Figure 3 shows the variation of MBE with COT among all samples, multi-layer clouds, single-layer clouds, ice clouds and water clouds of different satellites. The circle represents MBE, and the error bar represents Std. It can be seen from Figure 3a,b that the MBE of FY-4A and HIMWARI-8 is almost not affected by COT. For ice cloud and COT > 6, the MBE of HIMAWARI-8 decreases, and the MBE of FY-4A increases. It can be seen from Figure 3c that when COT is less than 7, the MBE between FY-4A and HIMAWARI-8 is hardly affected by COT, and MBE in different scenarios (multi-layer clouds, single-layer clouds, ice clouds, water clouds) is basically the same; when COT > 7, the MBE of single-layer cloud decreases with COT, and the error is larger than that of multi-layer cloud. For ice cloud and COT > 6, the MBE of HIMAWARI-8 and FY-4A changes in opposite directions, so the difference between HIMAWIRI-8 and FY-4A increases.

The variation between MBE with CTH among all samples, multi-layer clouds, single-layer clouds, ice clouds and water clouds of different satellites is shown in Figure 4. It can be seen from Figure 4a,b that when the CTH is less than 5 km, the MBE is greater than 0 and decreases with cloud top height; when the CTH is greater than 5 km, the MBE is less than 0 and decreases with cloud top height. The single-layer and multi-layer clouds of FY-4A and HIMAWARI-8 have basically the same MBE and Std at different cloud top heights, and the MBE of the two satellites has the same trend with the cloud top height. It can be seen from Figure 4c that the MBE of FY-4A and HIMWARI-8 is hardly affected by the number of layer and the cloud top height, but when COT > 6, the MBE of the ice cloud increases with COT, and the MBE of the water cloud decreases.

Before performing cloud phase recognition, one must judge whether there are clouds in the sky. The OCO-2 data in August 2016 were used for comparison with the CALIOP data. The samples selected according to latitude and longitude were from the 450 orbits during August 2016 over the Pacific Ocean.

The change in MBE between different satellites with cloud types (Ctypes) is shown in Figure 5. It can be seen from Figure 5 that the MBE varies with the cloud type in the same trend in the three cases. The MBE of FY-4A is less than HIMAWARI-8. The MBE between FY-4A and HIMAWARI-8 is less than 0. The difference between the first six cloud types is relatively small, and the difference between the 7th and 8th cloud types is greater. Among them, 0 represents low overcast, transparent, 1 represents low overcast, opaque, 2 represents transition stratocumulus, 3 represents low, broken cumulus,

4 represents altocumulus (transparent), 5 represents altostratus (opaque), 6 represents cirrus (transparent), and 7 represents deep convective (opaque).

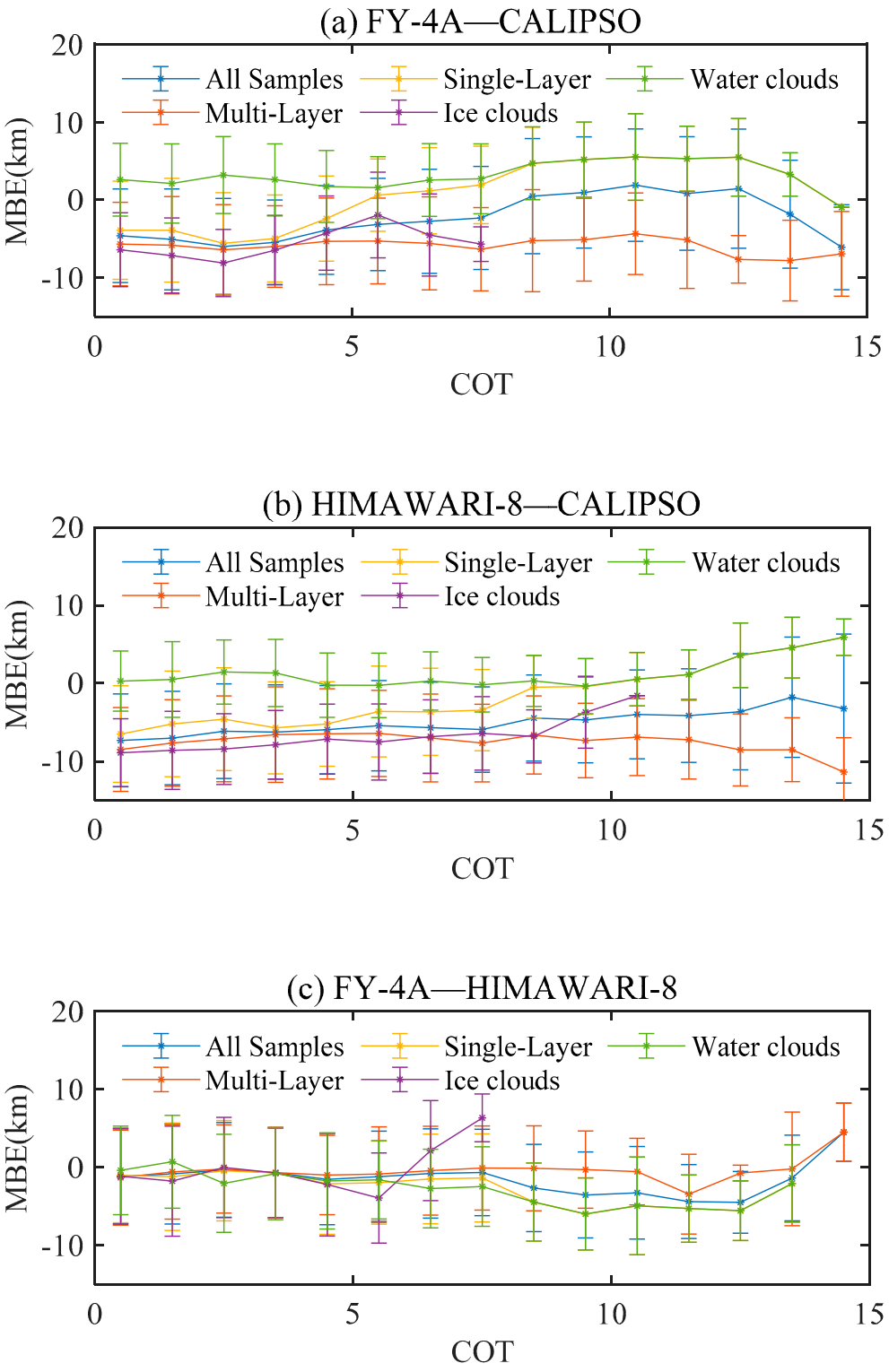


Figure 3. The variation of MBE with COT for all samples, multi-layer clouds, single-layer clouds, ice clouds and water clouds of different satellites. The error bars represent STD. (**a**) FY-4A–CALIPSO (**b**) HIMAWARI-8–CALIPSO (**c**) FY-4A–HIMAWARI-8.

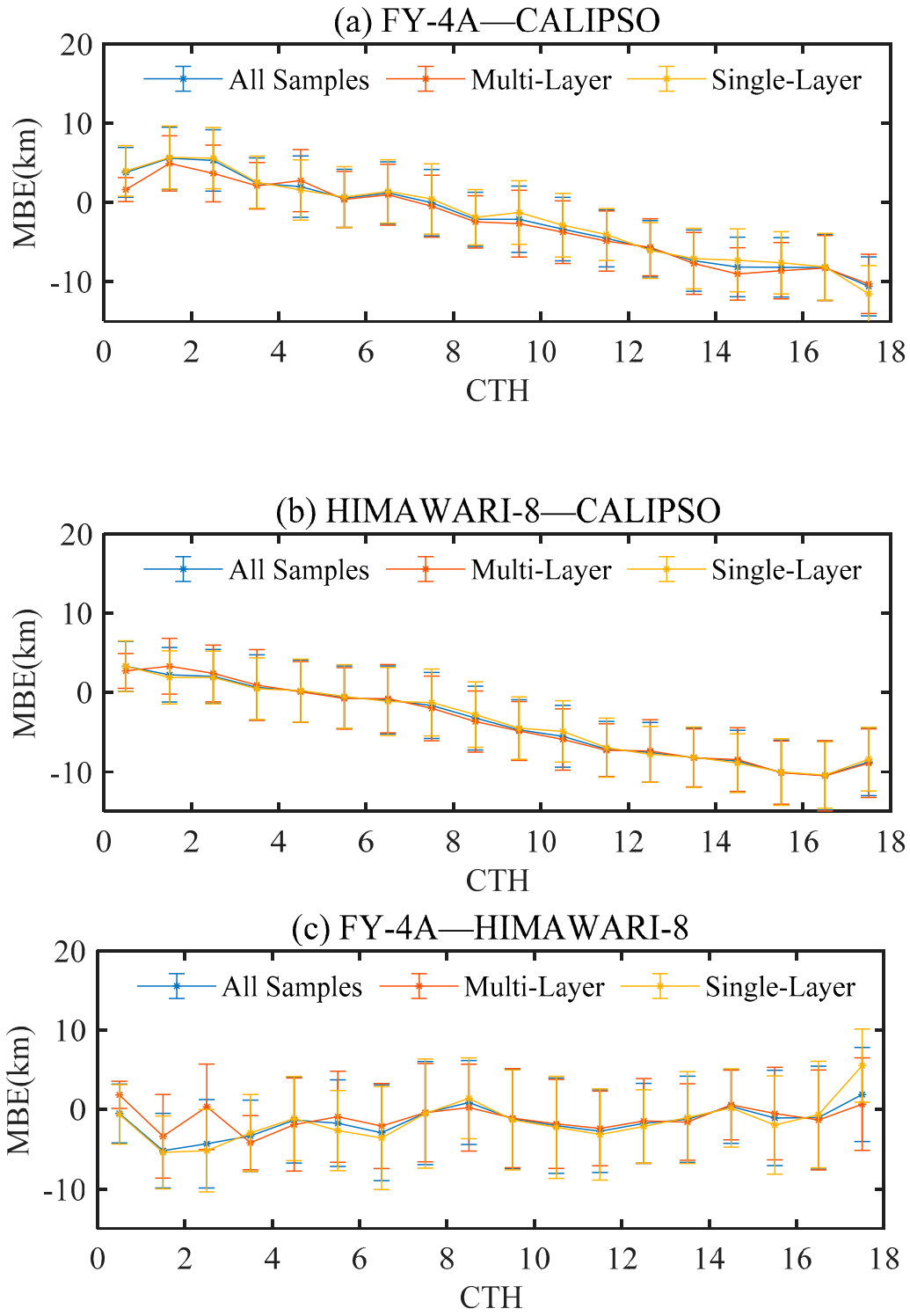


Figure 4. The variation of MBE with CTH for all samples, multi-layer clouds and single-layer clouds of different satellites. The error bars represent STD. (**a**) FY-4A–CALIPSO (**b**) HIMAWARI-8–CALIPSO (**c**) FY-4A–HIMAWARI-8.

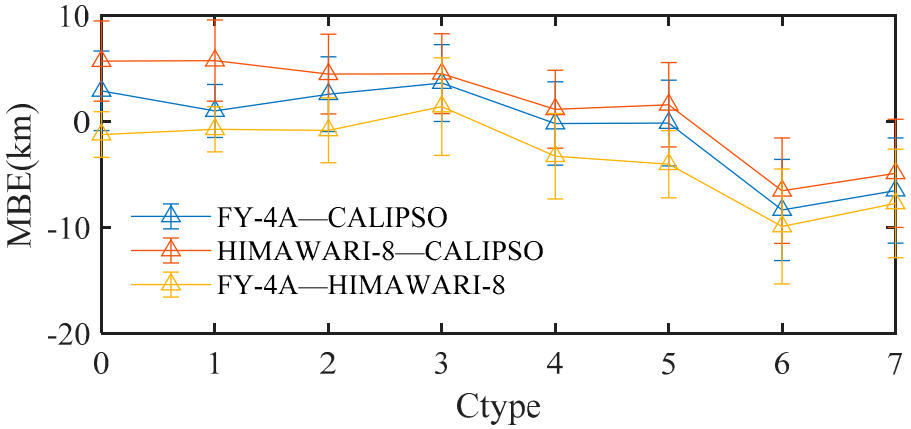


Figure 5. MBE between different satellites varies with cloud types. The error bars represent STD.

It can be seen from the above analysis that although the cloud top heights of FY-4A and HIMAWARI-8 have large errors, the consistency between the two is good, and the two can be used for joint observation. The optical thickness has little effect on the measurement of cloud top height of FY-4A and HIMAWARI-8, but when COT > 6, the MBE between FY-4A and HIMAWARI-8 of ice cloud increases with COT, the MBE of water cloud decreases. When the optical thickness is small, the consistency between FY-4A and HIMAWARI-8 is less affected by the optical thickness except for ice cloud. When COT < 6, the consistency of the ice cloud and water cloud are better and worse when COT > 6. When the optical thickness is large, FY-4A and HIMAWARI-8 single-layer clouds are more different than multi-layer clouds, that is, the consistency of multi-layer clouds is better than single-layer clouds. The cloud top height has a great influence on the measurement accuracy of FY-4A and HIMAWARI-8, but the consistency between the two is less affected by the cloud top height. The cloud type has effect on the measurement of cloud top height of FY-4A and HIMAWARI-8. The measurement error of altocumulus and altostratus is smaller and larger in other cloud types. The cloud type has a significant impact on the consistency between FY-4A and HIMWARI-8. The consistency of the cloud type is better in the first six types and worse in the latter two types.

3.2. The Problem of Missing Measurement of FY-4A and HIMAWARI-8

In addition to the accuracy of the geostationary satellite's measurement of cloud top height and the consistency between the two satellites, another factor that affects the joint observation of geostationary satellites is the problem of missing measurement of geostationary satellites. The missing rate is defined as the ratio of the number of samples where CALIPSO has cloud top height data, but FY-4A (HIMAWARI-8) does not to the number of samples where CALIPSO has cloud top height data. Figure 6 shows the missing rates of FY-4A and HIMAWARI-8 in different scenarios. It can be seen from Figure 6 that the missing rate of satellites under different cloud scenarios does not change much. The missing rate of HIMAWARI-8 is 0.6–0.8, and the missing rate of FY-4A is 0.2–0.4. Both FY-4A and HIMAWARI-8 have a large missing rate and the difference in the missing rate between the two is large. This is a huge challenge for the joint observation of FY-4A and HIMAWARI-8.

Figure 7 shows the variation of the frequency distribution of missing data in different cloud scenarios with COT. Figure 8 shows the frequency distribution of missing data in different cloud scenarios with CTH. As shown in the figure, although the missing samples are mainly concentrated in optically thin and high clouds, the missing rate is less affected by the optical thickness and cloud top height.

Figure 9 shows the missing rate of FY-4A and HIMAWARI-8 under different cloud types. It can be seen from the figure that the missing rate of HIMAWARI-8 is greater than that of FY-4A. The missing rate of FY-4A in cloud type 0 and 1 is higher than other cloud

types. The missing rate of HIMAWARI-8 in cloud type 3 and 6 is higher than other cloud types. The missing rate of the two satellites have different trends with cloud types.

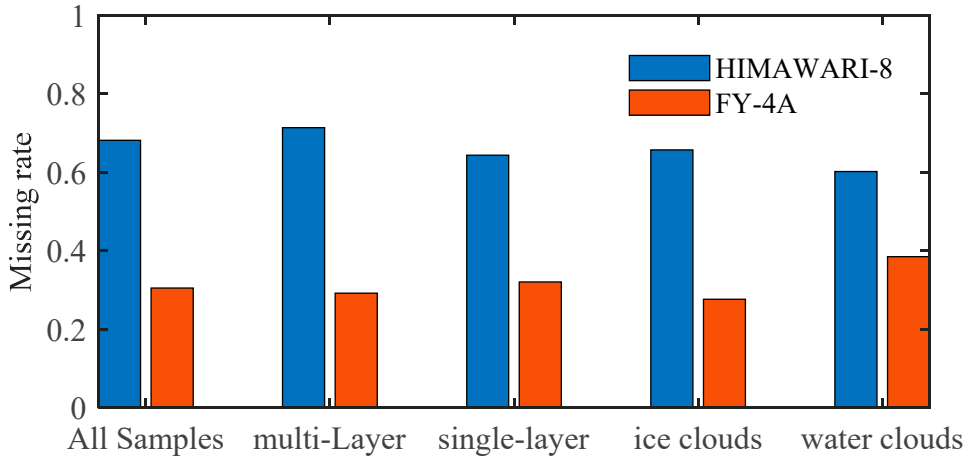


Figure 6. Missing rate of FY-4A and HIMWARI-8 in different scenarios.

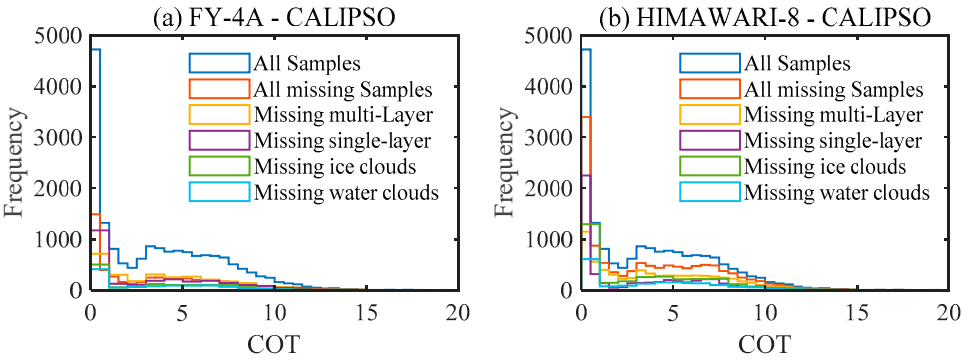


Figure 7. The frequency distribution of missing data of FY-4A and HIMAWARI-8 varies with COT. (**a**) FY-4A and (**b**) HIMAWARI-8.

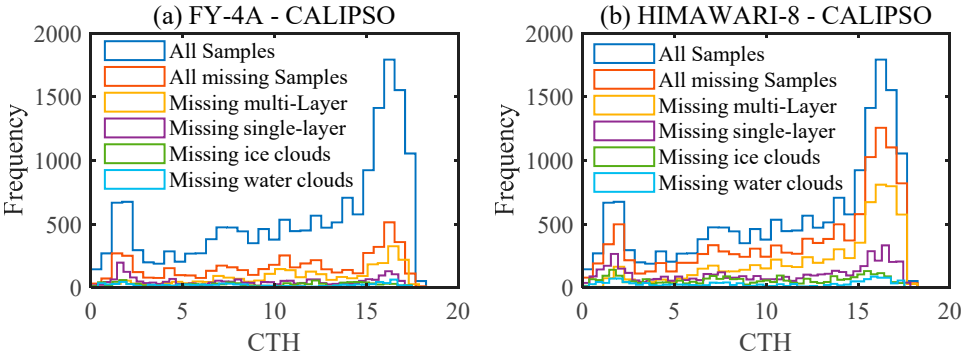


Figure 8. The frequency distribution of missing data of FY-4A and HIMAWARI-8 varies with CTH. (**a**) FY-4A and (**b**) HIMAWARI-8.

Table 2 shows the missing rates of FY-4A and HIMWARI-8 under different surface types. It can be seen from the table that the missing rate of FY-4A on land is slightly higher than that of water surface, and the missing rate of HIMAWARI-8 on land is lower than that of water surface, but there is no significant difference in the missing rate of the two satellites under the two surface types.

Table 2. Missing rate of FY-4A and HIMAWARI-8 under different surface types.

	Missing Rate	
	land	water
FY-4A	0.33	0.29
HIMAWARI-8	0.63	0.71

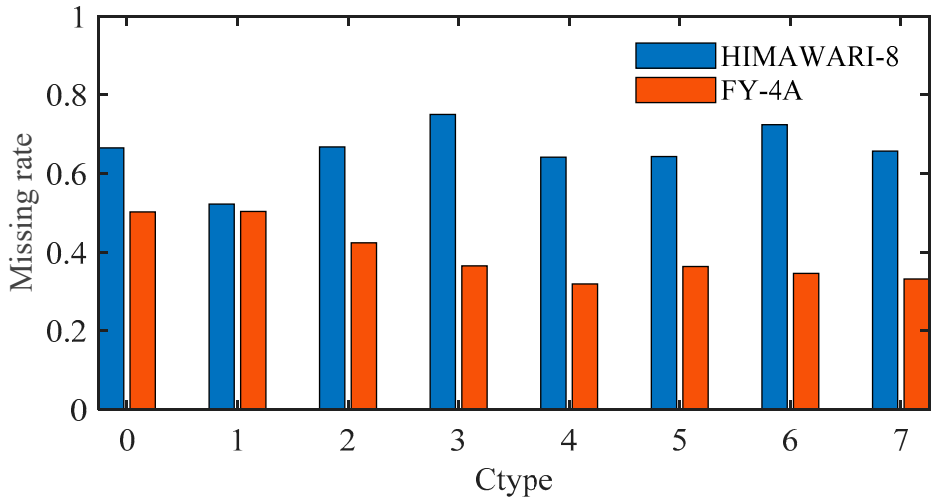


Figure 9. Missing rate of FY-4A and HIMWARI-8 under different cloud types: 0 represents low overcast, transparent, 1 represents low overcast, opaque, 2 represents transition stratocumulus, 3 represents low, broken cumulus, 4 represents altocumulus (transparent), 5 represents altostratus (opaque), 6 represents cirrus (transparent), and 7 represents deep convective (opaque).

4. Discussion

Since the ΔCTH frequency distribution of FY-4A and HIMAWARI-8 is similar and the consistency is good, FY-4A and HIMAWARI-8 can be jointly observed. However, the poor accuracy of cloud top height and the missing measurement of geostationary satellites are still important factors that limit the joint observation of geostationary satellites. The cloud top height error is mainly affected by the cloud top height and cloud type. The measurement consistency between FY-4A and HIMAWARI-8 is greatly affected by the cloud type. Therefore, it is very important to improve the accuracy of FY-4A and HIMAWARI-8 in measuring the cloud top height.

It can be seen from the above studies that FY-4A and HIMWARI-8 have a large missing rate, and the missing rate of HIMWARI-8 is greater than that of FY-4A. Cloud top height, optical thickness and surface type have no significant influence on the missing rate. Cloud type has effect on the missing rate FY-4A has a higher missing rate for cloud types 0 and 1 (low cloud), and HIMWARI-8 has a higher missing rate for cloud types 3 and 6 (low broken cloud and transparent cirrus cloud). There is a significant difference in the relationship between the missing rate of the two satellites and the cloud type.

5. Conclusions

In order to evaluate the reliability of the joint observations of FY-4 and HIMAWARI-8, we evaluated the accuracy of cloud top height of FY-4A and HIMAWARI-8 and the consistency between the two satellites and studied the problem of missing measurements of the two. The measurement results of FY-4A and HIAMWARI-8 are in good agreement, but the measurement error of the two is relatively large, and the measurement error of FY-4A is greater than that of HIMWARI-8. The error of cloud top height is affected by the cloud top height and cloud type, and the consistency of cloud top height between the two is mainly affected by the cloud type. Therefore, improving the accuracy of FY-4A and HIMAWARI-8's cloud top height is very important for the joint observation of the two.

The missing measurement of FY-4A and HIMAWARI-8 is also an important factor restricting the joint observation of FY-4A and HIMAWARI-8, and its missing rate is not almost unaffected by cloud top height, optical thickness and surface type. Cloud type has an effect on the missing rate. For FY-4A, the missing rate is higher for low overcast, transparent and low overcast, opaque clouds than other cloud types. However, HIMAWARI-8 has a higher missing rater for low, broken cumulus and cirrus than other cloud types. There is a significant difference in the relationship between the missing rate of the two satellites and the cloud type.

FY-4A and HIMAWARI-8 have good consistency and can be jointly observed, but the error and the problem of missing measurement of the satellite still limit the reliability of the joint observation of the geostationary satellite.

Author Contributions: All authors were involved in the design and discussion of the study. This research idea was conceived by X.S. and Q.L. The experiments were designed and conducted by Q.L. The data were analyzed and interpreted by Q.L. The manuscript was written by Q.L. and revised by X.S. and X.W. All authors have read and agreed to the published version of the manuscript.

Funding: This study was financially supported by the National Natural Science Foundation of China (NSFC) (grant no. 41575020).

Institutional Review Board Statement: Not applicable.

Informed Consent Statement: Not applicable.

Data Availability Statement: In this manuscript, we used two kinds of data, the data of CALIPSO (https://asdc.larc.nasa.gov/data/CALIPSO/LID_L2_05kmCLay-Standard-V4--20 (Accessed on 2 September 2021)), the data of FY-4A ("http://satellite.nsmc.org.cn/PortalSite/Data/DataView.aspx?SatelliteType=1&DataCategoryCode=Atmosphere&DataTypeCode=CTH" (Accessed on 2 September 2021)) and the data of HIMAWARI-8 ("ftp.ptree.jaxa.jp" (Accessed on 2 September 2021)).

Conflicts of Interest: The authors declare no conflict of interest.

References

1. Wetherald, R.T. Cloud Feedback Processes in a General Circulation Model. *J. Atmos.* **1988**, *45*, 1397–1416. [CrossRef]
2. Baker, M.B.; Peter, T. Small-scale cloud processes and climate. *Nature* **2008**, *451*, 299–300. [CrossRef] [PubMed]
3. Trenberth, K.E.; Fasullo, J.T.; Kiehl, J. Earth's Global Energy Budget. *Bull. Am. Meteorol. Soc.* **2009**, *90*, 311–323. [CrossRef]
4. Dessler, A.E. A Determination of the Cloud Feedback from Climate Variations over the Past Decade. *Science* **2010**, *330*, 1523–1527. [CrossRef] [PubMed]
5. Wang, H.; Su, W. Evaluating and understanding top of the atmosphere cloud radiative effects in Intergovernmental Panel on Climate Change (IPCC) Fifth Assessment Report (AR5) Coupled Model Intercomparison Project Phase 5 (CMIP5) models using satellite observations. *J. Geophys. Res. Atmos.* **2013**, *118*, 683–699. [CrossRef]
6. Stocker, T.; Plattner, G.K.; Dahe, Q. IPCC Climate Change 2013: The Physical Science Basis—Findings and Lessons Learned. In Proceedings of the Egu General Assembly Conference 2014, Vienna, Austria, 27 April–2 May 2014.
7. Niemel, S.; Risnen, P.; Savijrvi, H. Comparison of surface radiative flux parameterizations. *Atmos. Res.* **2001**, *58*, 141–154. [CrossRef]
8. Stephens, G.L.; Wild, M.; Stackhouse, P.W., Jr.; L'Ecuyer, T.; Kato, S.; Henderson, D.S. The Global Character of the Flux of Downward Longwave Radiation. *J. Clim.* **2012**, *25*, 2329–2340. [CrossRef]
9. Wang, K.; Dickinson, R.E. Global atmospheric downward longwave radiation at the surface from ground-based observations, satellite retrievals, and reanalyses. *Rev. Geophys.* **2013**, *51*, 150–185. [CrossRef]
10. Boucher, O.; Randall, D.; Artaxo, P.; Bretherton, C.; Feingold, G.; Forster, P.; Zhang, X.Y. Clouds and Aerosols. In *Climate Change 2013: The Physical Science Basis. Contribution of Working Group I to the Fifth Assessment Report of the Intergovernmental Panel on Climate Change*; Cambridge University Press: Cambridge, UK, 2013.
11. Merino, A.; Soriano, J.F.; Sánchez, J.; López, L.; Frias, M.R. Cloud top height estimation from WRF model: Application to the infrared camera onboard Euso-Balloon (CNES). In Proceedings of the 34th International Cosmic Ray Conference (ICRC2015), The Hague, The Netherlands, 30 July—6 August 2015.
12. Soriano, J.F.; Peral, L.D.; Ríos, J.A.M.d.L.; Prieto, H.; Frias, M.R. The Spanish Infrared Camera onboard the EUSO-Balloon (CNES) flight on 24 August 2014. In Proceedings of the 34th International Cosmic Ray Conference (ICRC2015), The Hague, The Netherlands, 30 July–6 August 2015.
13. Danne, O.; Quante, M.; Raschke, E.; Weitkamp, C. Investigations of cloud layer base and top heights from 95 GHz radar reflectivity data. *Phys. Chem. Earth Part B Hydrol. Ocean. Atmos.* **1999**, *24*, 167–171. [CrossRef]

14. Krofli, R.A.; Kelly, R.D. Meteorological research applications of MM-wave radar. *Meteorol. Atmos. Phys.* **1996**, *59*, 105–121. [CrossRef]
15. Hollars, S.; Qiang, F.; Comstock, J.; Ackerman, T. Comparison of cloud-top height retrievals from ground-based 35 GHz MMCR and GMS-5 satellite observations at ARM TWP Manus site. *Atmos. Res.* **2004**, *72*, 169–186. [CrossRef]
16. Platnick, S.; King, M.D.; Ackerman, S.A.; Menzel, W.P.; Baum, B.A.; Riédi, J.C.; Frey, R.A. The MODIS cloud products: Algorithms and examples from Terra. *IEEE Trans. Geosci. Remote Sens.* **2003**, *41*, 459–473. [CrossRef]
17. Minnis, P.; Sun-Mack, S.; Young, D.F.; Heck, P.W.; Garber, D.P.; Chen, Y.; Spangenberg, D.A.; Arduini, R.F.; Trepte, Q.Z.; Smith, W.L.; et al. CERES Edition-2 Cloud Property Retrievals Using TRMM VIRS and Terra and Aqua MODIS Data—Part I: Algorithms. *IEEE Trans. Geosci. Remote Sens.* **2011**, *49*, 4374–4400. [CrossRef]
18. Schmit, T.J.; Gunshor, M.M.; Menzel, W.P.; Gurka, J.J.; Bachmeier, A.S. Introducing the next-generation Advanced Baseline Imager on GOES-R. *Bull. Am. Meteorol. Soc.* **2005**, *86*, 8. [CrossRef]
19. Campbell, J.R.; Dolinar, E.K.; Lolli, S.; Fochesatto, G.J.; Gu, Y.; Lewis, J.R.; Marquis, J.W.; McHardy, T.M.; Ryglicki, D.R.; Welton, E.J. Cirrus Cloud Top-of-the-Atmosphere Net Daytime Forcing in the Alaskan Subarctic from Ground-Based MPLNET Monitoring. *J. Appl. Meteorol. Climatol.* **2020**, *60*, 51–63. [CrossRef]
20. Winker, D.M.; Vaughan, M.A.; Omar, A.; Hu, Y.; Powell, K.A.; Liu, Z.; Hunt, W.H.; Young, S.A. Overview of the CALIPSO Mission and CALIOP Data Processing Algorithms. *J. Atmos. Ocean. Technol.* **2009**, *26*, 2310–2323. [CrossRef]
21. Min, M.; Wang, P.; Campbell, J.R.; Zong, X.; Xia, J. Cirrus Cloud Macrophysical and Optical Properties over North China from CALIOP Measurements. *Adv. Atmos. Sci.* **2011**, *3*, 653–664. [CrossRef]
22. Stephens, G.L.; Vane, D.G.; Boain, R.J.; Mace, G.G.; Sassen, K.; Wang, Z.; Illingworth, A.J.; O'connor, E.J.; Rossow, W.B.; Durden, S.L.; et al. The Cloudsat Mission and The A-Train. *Bull. Am. Meteorol. Soc.* **2002**, *83*, 1771–1790. [CrossRef]
23. Da, C. Preliminary assessment of the Advanced Himawari Imager (AHI) measurement onboard Himawari-8 geostationary satellite. *Remote Sens. Lett.* **2015**, *6*, 637–646. [CrossRef]
24. Liu, Q.; Li, Y.; Yu, M.; Long, S.C.; Yang, C. Daytime Rainy Cloud Detection and Convective Precipitation Delineation Based on a Deep Neural Network Method Using GOES-16 ABI Images. *Remote Sens.* **2019**, *11*, 2555. [CrossRef]
25. Schmetz, J.; Holmlund, K.; Hoffman, J.; Strauss, B.; Mason, B.; Gaertner, V.; Koch, A.; Van De Berg, L. Operational Cloud-Motion Winds from Meteosat Infrared Images. *J. Appl. Meteorol.* **1993**, *32*, 1206–1225. [CrossRef]
26. Smith, W.L. An improved method for calculating tropospheric temperature and moisture profiles from satellite radiometer measurements. *Mon. Weather Rev.* **2009**, *96*, 387–396. [CrossRef]
27. Frey, R.A.; Baum, B.A.; Menzel, W.P.; Ackerman, S.A.; Moeller, C.C.; Spinhirne, J.D. A comparison of cloud top heights computed from airborne lidar and MAS radiance data using CO_2 slicing. *J. Geophys. Res. Atmos.* **1999**, *104*, D20. [CrossRef]
28. Min, M.; Wu, C.; Li, C.; Liu, H.; Xu, N.; Wu, X.; Chen, L.; Wang, F.; Sun, F.; Qin, D.; et al. Developing the Science Product Algorithm Testbed for Chinese Next-Generation Geostationary Meteorological Satellites: Fengyun-4 Series. *J. Meteorol. Res.* **2017**, *31*, 708–719. [CrossRef]
29. Iwabuchi, H.; Saito, M.; Tokoro, Y.; Putri, N.S.; Sekiguchi, M. Retrieval of radiative and microphysical properties of clouds from multispectral infrared measurements. *Prog. Earth Planet. Sci.* **2016**, *3*, 32. [CrossRef]
30. Menzel, W.P.; Frey, R.A.; Zhang, H.; Wylie, D.P.; Moeller, C.C.; Holz, R.E.; Maddux, B.; Baum, B.A.; Strabala, K.I.; Gumley, L.E. MODIS Global Cloud-Top Pressure and Amount Estimation: Algorithm Description and Results. *J. Appl. Meteorol. Climatol.* **2008**, *47*, 1175–1198. [CrossRef]
31. Heidinger, A.K.; Pavolonis, M.J. Gazing at Cirrus Clouds for 25 Years through a Split Window. Part I: Methodology. *J. Appl. Meteorol. Climatol.* **2009**, *48*, 6. [CrossRef]
32. Li, J.; Menzel, W.P.; Schreiner, A.J. Variational Retrieval of Cloud Parameters from GOES Sounder Longwave Cloudy Radiance Measurements. *J. Appl. Meteorol.* **2001**, *40*, 312–330. [CrossRef]
33. Iwabuchi, H.; Putri, N.S.; Saito, M.; Tokoro, Y.; Sekiguchi, M.; Yang, P.; Baum, B.A. Cloud Property Retrieval from Multiband Infrared Measurements by Himawari-8. *J. Meteorol. Soc. Jpn. Ser. II* **2017**, *96*, 27–42. [CrossRef]
34. Liu, Z.; Vaughan, M.; Winker, D.; Kittaka, C.; Getzewich, B.; Kuehn, R. The CALIPSO Lidar Cloud and Aerosol Discrimination: Version 2 Algorithm and Initial Assessment of Performance. *J. Atmos. Ocean. Technol.* **2009**, *26*, 1198–1213. [CrossRef]
35. Vaughan, M.A.; Powell, K.A.; Winker, D.M.; Hostetler, C.A.; Kuehn, R.E.; Hunt, W.H.; Getzewich, B.J.; Young, S.A.; Liu, Z.; McGill, M.J. Fully Automated Detection of Cloud and Aerosol Layers in the CALIPSO Lidar Measurements. *J. Atmos. Ocean. Technol.* **2008**, *26*, 2034–2050. [CrossRef]
36. Hu, Y.; Winker, D.; Vaughan, M.; Lin, B.; Omar, A.; Trepte, C.; Kuehn, R. CALIPSO/CALIOP Cloud Phase Discrimination Algorithm. *J. Atmos. Ocean. Technol.* **2009**, *26*, 2293–2309. [CrossRef]